Ann. Acad. Rom. Sci.
Ser. Math. Appl.
ISSN 2066-6594 Vol. 17, No. 3/2025

EXPLICIT SOLUTIONS OF THE QUADRATICALLY CLOSED FOLGAR-TUCKER EQUATION IN A THREE DIMENSIONAL PLANAR FLOW*

Christina Papenfuss† Maedeh Ranjbar‡

Dedicated to Prof. Liliana Restuccia on the occasion of her 70th anniversary

DOI 10.56082/annalsarscimath.2025.3.293

Abstract

During the mold-filling process, the fiber orientation in a flowing fiber suspension plays a crucial role in determining the material properties of the resulting fiber composite. A common modelling approach introduces the second-order orientation tensor governed by the Folgar–Tucker equation, which serves as the equation of motion, combined with an appropriate closure relation. In the present work, analytical solutions in three dimensions of the quadratically closed Folgar–Tucker equation are presented for a planar flow. The analysis reveals that the solution does not reduce to a purely two-dimensional orientation tensor. However, in the long-term limit, only two components of the orientation tensor remain independent—corresponding to the same number as in the two-dimensional case. A reconstruction of the orientation distribution function (ODF) further highlights the distinction between the fully three-dimensional orientation state and the effectively two-dimensional assumption in steady flow conditions. The analytical solution also shows that the steady-state orientation is highly sensitive to

*Accepted for publication on November 04, 2025

†Christina.Papenfuss@HTW-Berlin.de, Hochschule für Technik und Wirtschaft Berlin, Wilhelminenhofstraße 75A, 12459 Berlin, Germany

‡Maedeh.Ranjbar@htw-berlin.de, Hochschule für Technik und Wirtschaft Berlin, 12459 Berlin, Germany

the shear rate. At very low shear rates the solution is nearly isotropic orientation tensor, whereas at very high shear rates it approaches a configuration that is strongly aligned in the velocity direction.

Keywords: Folgar-Tucker equation, analytical solution, planar flow, fiber suspension, orientation tensor, Couette flow.
MSC: 76T20, 34A05.

1 Introduction

Alignment phenomena in suspensions of short, rigid fibers play a critical role in numerous industrial processes. In a flow process, the local distribution of fiber orientations depends on the shear rate and the flow geometry. Notably, fiber orientation significantly influences the mechanical properties of fiber composite materials, such as fiber-reinforced concrete produced by pouring, or fiber-reinforced polymers after injection molding. Once set, the fiber alignment is preserved, directly affecting the final properties of the composite. Therefore, accurately predicting and controlling fiber orientation during manufacturing is essential for optimizing material performance. As demands for efficient material and energy use grow, the ability to guide fiber alignment becomes increasingly vital for future engineering applications.

In a coarsened description orientation tensors are introduced as a measure of orientational order. A widely used model equation for the second order orientation tensor in a flowing fiber suspension is the Folgar-Tucker equation (FTE). Analytical solutions of the FTE have rarely been discussed in the literature, despite their potential to provide fundamental insight and to serve as validation benchmarks for numerical schemes.

This work addresses that gap for a simple flow geometry - a three-dimensional planar flow. Our method follows the approach described in [1]. Section 2 introduces the orientation distribution function, orientation tensors, and the Folgar–Tucker equation. Section 3 details the reduction of the nonlinear FTE to a linear problem and its application to three-dimensional planar flow. Analytical solutions are presented and discussed in Section 4, and the paper concludes with a summary of results in Section 5.

2 Orientation tensors and the Folgar-Tucker equation

In our model, the fibers are idealized as rigid, slender bodies of infinite aspect ratio.

The orientations of fiber particles can be described by an orientation distribution function defined on the unit sphere. Conceptually, one may imagine all particles within a representative volume element having their centers of mass fixed at the center of a unit sphere. The endpoints of the particles - scaled to a length of two - then define a spatial distribution on the sphere's surface. The ODF represents the probability density of finding a particle aligned in a particular direction $\boldsymbol{n}$, where $\boldsymbol{n}$ is a unit vector. If all orientations are equally probable, the distribution is homogeneous, corresponding to an isotropic state. Conversely, if there is a preferred orientation, the ODF exhibits a concentration around that direction, characterizing an anisotropic distribution.

Because the full orientation distribution is generally not accessible through direct measurement and is difficult to handle in numerical simulations, moments of the distribution function are introduced to capture its essential features in a more tractable form [2, 3]. The symmetric tensors

$$\boldsymbol{A}^{(k)}(\boldsymbol{x},t) := \int_{S^2} f(\boldsymbol{x},t,\boldsymbol{n})\, \underbrace{\boldsymbol{n}\dots\boldsymbol{n}}_{\text{k times}}\, d^2n \tag{1}$$

are referred to as orientation tensors. They are fully symmetric tensors of order k and have trace one. As macroscopic quantities, they do not depend on the microscopic fiber orientation $\boldsymbol{n}$. In practice, usually only the second order tensor is retained as a state variable.

From the infinite hierarchy of orientation tensors the ODF can be reconstructed [4]:

$$f(\boldsymbol{x},t,\boldsymbol{n}) = \frac{1}{4\pi}\left(1 + \sum_{\text{l even}} \frac{(2l+1)!!}{l!}\ \overline{A_{\mu 1\dots\mu l}(\boldsymbol{x},t)}\ \overline{n_{\mu 1}\dots n_{\mu l}}\right)\ . \tag{2}$$

By $\overline{\quad\quad}$ we denoted the symmetric traceless part of a tensor. The scalar products between $\overline{\boldsymbol{A}}$ and $\overline{\boldsymbol{n}\dots\boldsymbol{n}}$ have been written in components and $l!! = l(l-2)(l-4)\cdots$.

Neglecting the higher order orientation tensors yields the following approximation

$$f(\boldsymbol{x},t,\boldsymbol{n}) \approx \frac{1}{4\pi}\left(1 + \frac{15}{2}\ \overline{A_{ij}(\boldsymbol{x},t)}\ \overline{n_i n_j}\right)\ . \tag{3}$$

One can show that, in two dimensions, the orientation distribution function reduces to:

$$f(\boldsymbol{x}, t, \boldsymbol{n}) \approx \frac{1}{2\pi}\left(1 + 4 \ \overline{A_{ij}(\boldsymbol{x}, t)} \ \overline{n_i n_j}\right) \ . \tag{4}$$

The FTE for the evolution in time of the orientation tensor of second order is based on Jeffery's equation [5] for the orientation of a single fiber in the flow field supplemented by an orientation-diffusion term that represents inter-fiber collisions. In three dimensions, the equation can be written as [3]

$$\frac{\mathrm{d}\boldsymbol{A}}{\mathrm{d}t} = \boldsymbol{A} \cdot \nabla \boldsymbol{u} + (\nabla \boldsymbol{u})^T \cdot \boldsymbol{A} - 2\nabla \boldsymbol{u} : \boldsymbol{A}^{(4)} + 2D_r(\mathbf{1} - 3\boldsymbol{A}), \tag{5}$$

where $\boldsymbol{u}$ is the material velocity, $D_r > 0$ is a material parameter, $\mathbf{1}$ is the unit tensor, and ∇u denotes the velocity gradient with components $(\nabla u)_{ij} = \partial u_j / \partial x_i$.

The fourth order orientation tensor $\boldsymbol{A}^{(4)}$ appears in the equation governing the second-order tensor and must therefore be eliminated through a closure relation. For comparisons of different closure approaches, see, for example, [6, 7, 8, 9]).

Throughout this paper we adopt the quadratic closure, a dyadic product of second order orientation tensors,

$$\boldsymbol{A}^{(4)} = \boldsymbol{A}\boldsymbol{A}, \tag{6}$$

originally introduced by Doi [10]. Accordingly, we work with the quadratically closed Folgar–Tucker equation (FTE).

$$\frac{\mathrm{d}\boldsymbol{A}}{\mathrm{d}t} = \boldsymbol{A} \cdot \nabla \boldsymbol{u} + (\nabla \boldsymbol{u})^T \cdot \boldsymbol{A} - 2\nabla \boldsymbol{u} : \boldsymbol{A}\boldsymbol{A} + 2D_r(\mathbf{1} - 3\boldsymbol{A}). \tag{7}$$

3 Reduction to a linear problem and application to a planar flow

Following the method presented in [1], the nonlinear equation (7) can be reduced to a linear problem. Introduce an auxiliary symmetric second-order tensor $\boldsymbol{X}$ such that

$$\boldsymbol{A} = \frac{\boldsymbol{X}}{\operatorname{tr} \boldsymbol{X}}. \tag{8}$$

If $\boldsymbol{X}$ satisfies the linear differential equation

$$\frac{\mathrm{d}\boldsymbol{X}}{\mathrm{d}t} = \boldsymbol{X} \cdot \nabla \boldsymbol{u} + (\nabla \boldsymbol{u})^T \cdot \boldsymbol{X} + 2D_r(\mathbf{1}\,\mathrm{tr}(\boldsymbol{X}) - 3\boldsymbol{X}), \tag{9}$$

then $\boldsymbol{A}$ is a solution of (7) and automatically has unit trace.

3.1 Planar flow

Consider a planar flow in three dimensions with velocity in x-direction proportional to the y-coordinate, $v_x = \dot{\gamma} y$ commonly referred to as Couette flow. All vector and tensor components are expressed in a Cartesian coordinate system. The velocity field is steady in time.

The auxiliary tensor $\boldsymbol{X}$ and the velocity gradient are represented as

$$\boldsymbol{X} \equiv \begin{pmatrix} x & y & a \\ y & z & b \\ a & b & c \end{pmatrix}, \qquad \nabla \boldsymbol{u} \equiv \begin{pmatrix} 0 & 0 & 0 \\ \dot{\gamma} & 0 & 0 \\ 0 & 0 & 0 \end{pmatrix}. \tag{10}$$

Substituting these forms into equation (9) yields the system of first-order ordinary differential equations

$$\dot{x} = 2\dot{\gamma}\, y + 6D_r\left(\frac{x+z+c}{3} - x\right), \tag{11}$$

$$\dot{y} = \dot{\gamma}\, z - 6D_r\, y, \tag{12}$$

$$\dot{a} = \dot{\gamma}\, b - 6D_r\, a, \tag{13}$$

$$\dot{z} = 6D_r\left(\frac{x+z+c}{3} - z\right), \tag{14}$$

$$\dot{b} = -6D_r\, b, \tag{15}$$

$$\dot{c} = 6D_r\left(\frac{x+z+c}{3} - c\right) \tag{16}$$

with initial conditions $x(0) = x_0$, $y(0) = y_0$, $a(0) = a_0$, $z(0) = z_0$, $b(0) = b_0$, $c(0) = c_0$.

4 Analytical solutions

Equations (13) and (15) can be solved directly:

$$b(t) = b_0 e^{-6D_r t} \tag{17}$$

and

$$\dot{a}(t) = \dot{\gamma} b_0 e^{-6D_r t} - 6D_r a(t) \tag{18}$$

which gives

$$a(t) = e^{-6D_r t} \left(a_0 + \dot{\gamma} b_0 t \right). \tag{19}$$

From equations (14) and (16) we obtain

$$(z(t) - c(t))^{\cdot} = -6D_r(z(t) - c(t)) \tag{20}$$

hence

$$z(t) - c(t) = (z_0 - c_0)e^{-6D_r t}. \tag{21}$$

4.1 Long-term behavior

Equations (17), (19) and (21) imply the limits

$$\lim_{t\to\infty} b(t) = 0 \ , \quad \lim_{t\to\infty} a(t) = 0 \ , \quad \lim_{t\to\infty} z(t) = \lim_{t\to\infty} c(t) \ . \tag{22}$$

The auxiliary tensor approaches the form

$$\lim_{t\to\infty} \boldsymbol{X}(t) = \begin{pmatrix} x & y & 0 \\ y & z & 0 \\ 0 & 0 & z \end{pmatrix} \tag{23}$$

and the corresponding orientation tensor becomes

$$\lim_{t\to\infty} \boldsymbol{A}(t) = \begin{pmatrix} A_{11} & A_{12} & 0 \\ A_{12} & A_{22} & 0 \\ 0 & 0 & A_{22} \end{pmatrix}. \tag{24}$$

This stationary form coincides with the result reported in [11] for the quadratically closed FTE in the case of slender fibers (infinite aspect ratio). The orientation tensor is not purely two-dimensional, because $A_{33} \neq 0$; however, it possesses only two independent components, as in the two-dimensional case.

4.2 Solution for the remaining components

After substituting the solutions equations (17), (19) and (21), there remain three differential equations for the components $x(t)$, $y(t)$ and $z(t)$ of $\boldsymbol{X}(t)$. We introduce the auxiliary scalar quantities:

$$s(t) = x(t) + z(t) + c(t), \qquad r(t) = x(t) - \frac{z(t) + c(t)}{2}. \tag{25}$$

and the remaining three equations for (y, r, s) become

$$\frac{d}{dt}\begin{pmatrix} y(t) \\ r(t) \\ s(t) \end{pmatrix} = \underbrace{\begin{pmatrix} -6D_r & -\frac{\dot\gamma}{3} & \frac{\dot\gamma}{3} \\ 2\dot\gamma & -6D_r & 0 \\ 2\dot\gamma & 0 & 0 \end{pmatrix}}_{\boldsymbol{B}} \begin{pmatrix} y(t) \\ r(t) \\ s(t) \end{pmatrix} + \underbrace{\begin{pmatrix} \frac{\dot\gamma}{2} d_0\, e^{-6D_r t} \\ 0 \\ 0 \end{pmatrix}}_{f(t)}. \tag{26}$$

We denote the system matrix by $\boldsymbol{B}$.

A **particular solution** of the inhomogeneous system (26) is of the form $\mathbf{p}\, e^{-\mu t}$, where $\mathbf{p}$ satisfies the equations

$$(-6D_r \mathbf{1} - \mathbf{B}) \cdot \mathbf{p} = \mathbf{f}_0, \qquad \mathbf{f}_0 = \begin{pmatrix} \frac{\dot\gamma}{2} d_0 \\ 0 \\ 0 \end{pmatrix}.$$

The **eigenvalues** of the system matrix $\boldsymbol{B}$ may be found from the characteristic polynomial

$$P(\lambda) = \lambda^3 + 12D_r\lambda^2 + 36D_r^2\lambda - 4D_r\dot\gamma^2 \tag{27}$$

$$\tag{28}$$

with Cardano's formula. As the velocity gradient field has an antisymmetric part, the spectrum consists of one real eigenvalue and a pair of complex-conjugate eigenvalues, see [1]

$$\lambda_1 \in \mathbb{R}, \lambda_{2,3} = \beta \pm i\delta. \tag{29}$$

We reason analogously to [1]: The characteristic equation can be written as

$$\begin{aligned} P(\lambda) = 0 \quad \Longleftrightarrow \quad \lambda^3 + 12D_r\lambda^2 + 36D_r^2\lambda &= 4D_r\dot\gamma^2 \\ \lambda\,(6D_r + \lambda)^2 &= 4D_r\dot\gamma^2. \end{aligned} \tag{30}$$

The left-hand side of equation (30) vanishes for $\lambda = 0$ and is strictly increasing for $\lambda > 0$. The right hand side is always positive. Consequently there exists exactly one positive real root λ of equation (30). Because the trace of $\boldsymbol{B}$ is negative, the remaining two eigenvalues have negative real parts. The two complex eigenvalues cause the components of $\boldsymbol{X}$ to oscillate with exponential decay.

General solution

The homogeneous solution is obtained by diagonalizing the system matrix $\boldsymbol{B}$:

$$\boldsymbol{B} \cdot \mathbf{v}_j = \lambda_j \mathbf{v}_j, \qquad j = 1, 2, 3,$$

with eigenvalues λ_j and eigenvectors $\mathbf{v}_j$ and expanding $(y(t), r(t), s(t))^T = \sum_j C_j \mathbf{v}_j e^{\lambda_j t}$.

The full solution therefore reads

$$\begin{pmatrix} y \\ r \\ s \end{pmatrix} (t) = \sum_{j=1}^{3} \mathbf{v}_j \, C_j \, e^{\lambda_j t} + \mathbf{p} \, e^{-6D_r t}. \tag{31}$$

Reconstruction of tensor components

From $(y(t), r(t), s(t))$ the remaining components of $\boldsymbol{X}(t)$ are calculated as

$$x(t) = \tfrac{1}{3}\big(s(t) + 2r(t)\big), \tag{32}$$

$$z(t) = \tfrac{1}{3}\big(s(t) - r(t)\big) + \tfrac{1}{2}d(t), \tag{33}$$

$$c(t) = \tfrac{1}{3}\big(s(t) - r(t)\big) - \tfrac{1}{2}d(t). \tag{34}$$

Solution for the orientation tensor

Finally, the normalized tensor

$$\boxed{\boldsymbol{A}(t) = \frac{\boldsymbol{X}(t)}{\operatorname{tr} \boldsymbol{X}(t)}}$$

is the analytical solution of the nonlinear FTE.

4.3 Case study

In the following we consider solutions of equation (26) with initial value

$$\boldsymbol{X}(0) \equiv \begin{pmatrix} 1 & 0 & 0 \\ 0 & 1 & 0 \\ 0 & 0 & 1 \end{pmatrix}, \tag{35}$$

corresponding to an isotropic initial orientation tensor $\boldsymbol{A} = \frac{1}{3}\boldsymbol{I}$.

The orientation tensor components as a function of time are shown in figure 1 for three different shear rates: $\dot{\gamma} = 0.1,\ 1,\ 50\ (\mathrm{s}^{-1})$. The results show that $A_{22} = A_{33}$ and $A_{13} = A_{23} = 0$. Furthermore, A_{11} exhibits an increasing trend over time, while A_{22} decreases. It is also evident that the system reaches its steady state much faster at higher strain rates. The steady-state values of the orientation tensor for three representative shear rates are reported in Table 1.

Table 1: Steady-state orientation tensors A_∞ for different shear rates $\dot{\gamma}$.

$\dot{\gamma}(\mathrm{s}^{-1})$	0.1	1	50
A_∞	$\begin{pmatrix} 0.600573 & 0.200639 & 0 \\ 0.200639 & 0.199714 & 0 \\ 0 & 0 & 0.199714 \end{pmatrix}$	$\begin{pmatrix} 0.889871 & 0.151605 & 0 \\ 0.151605 & 0.055065 & 0 \\ 0 & 0 & 0.055065 \end{pmatrix}$	$\begin{pmatrix} 0.991419 & 0.046017 & 0 \\ 0.046017 & 0.004290 & 0 \\ 0 & 0 & 0.004290 \end{pmatrix}$

4.4 Validity of the 2D approximation

A central question for the practical use of orientation tensor models is under which conditions the three–dimensional orientation distribution can be approximated by its two–dimensional counterpart. This approximation is attractive because the 2D model is computationally less expensive and often sufficient for preliminary material design.

From the analytical solution with isotropic initial conditions obtained in the previous section, we observe that the out–of–plane components satisfy $A_{13} = A_{23} = 0$ for all times. Moreover, the component A_{33} decreases rapidly with increasing shear rate. The evolution of A_{11} as a function of $\dot{\gamma}$ (see Figure 2) shows that, for sufficiently large shear rates, A_{11} approaches 1. Since $\mathrm{tr}(\mathbf{A}) = 1$, this implies that $A_{22} = A_{33} \approx 0$ and, therefore, the 3D orientation state becomes effectively planar. In such cases, the 2D approximation becomes valid.

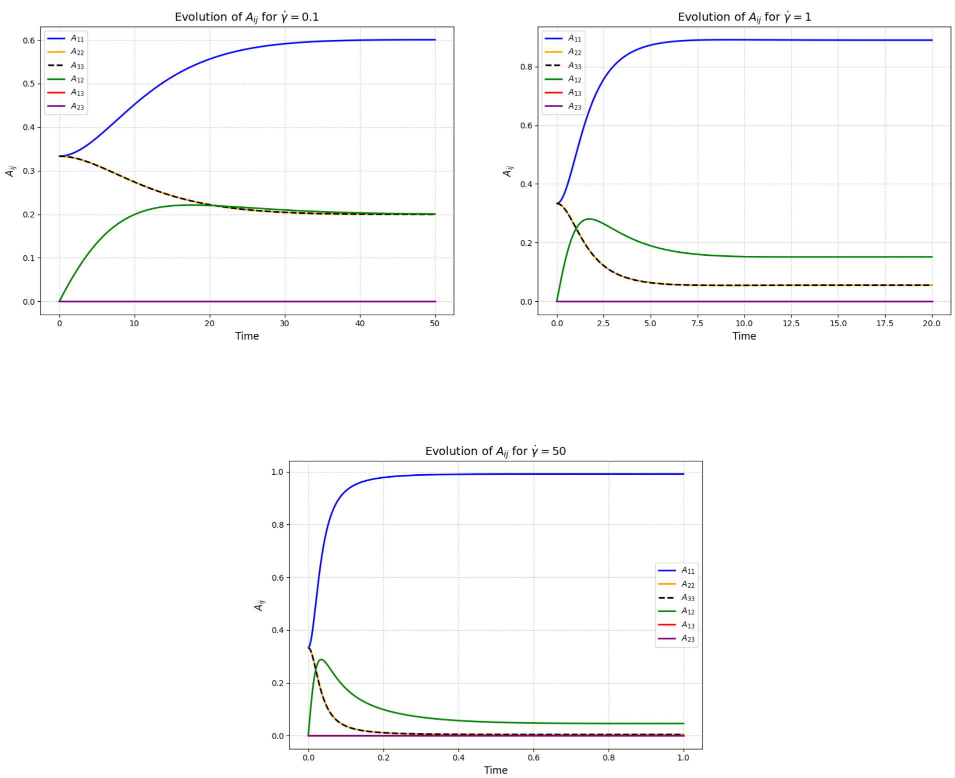

Figure 1: Orientation tensor components as a function of time for three different shear rates: $\dot{\gamma} = 0.1,\ 1,\ 50$ (s^{-1}).

For $D_r = 0.01$, the shear rates for which $A_{22} = A_{33} < 10^{-3}$ are approximately $\dot{\gamma} \geq 464\ \mathrm{s}^{-1}$. In this regime, the steady–state tensor takes the form of

$$\mathbf{A} \approx \begin{pmatrix} 0.9998 & 0.01708 & 0 \\ 0.01708 & 0.000584 & 0 \\ 0 & 0 & 0.000584 \end{pmatrix},$$

which corresponds to a highly anisotropic configuration in which the fibers are essentially aligned with the x–axis.

On the other hand, for sufficiently small shear rates, the orientation remains almost isotropic. For $D_r = 0.01$, the shear rates for which $|A_{22} - 1/3| < 10^{-3}$ are approximately $\dot{\gamma} \leq 0.002\ \mathrm{s}^{-1}$ and the tensor approaches

$$\mathbf{A} \approx \begin{pmatrix} 0.333 & 0.003 & 0 \\ 0.003 & 0.333 & 0 \\ 0 & 0 & 0.333 \end{pmatrix}.$$

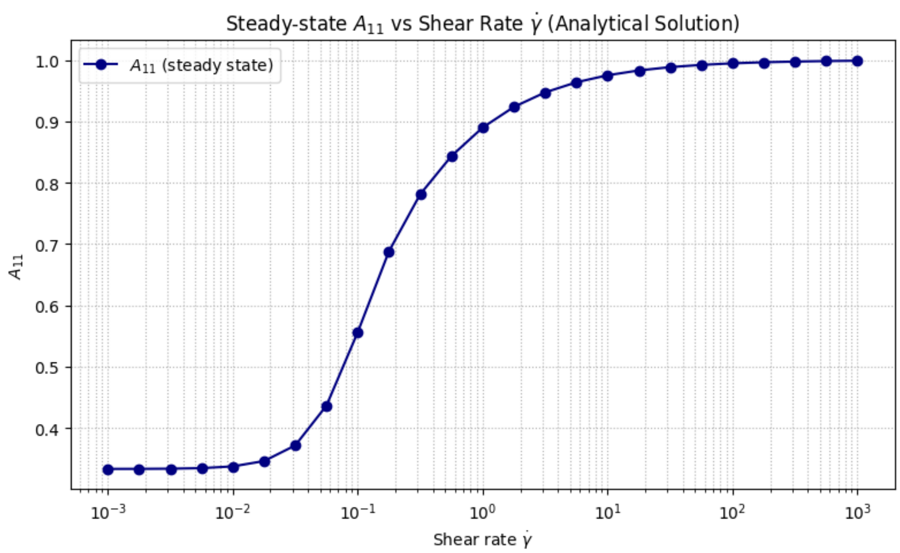

Figure 2: The orientation tensor component A_{11} in the steady state as a function of the shear rate.

The orientation distribution functions in 2D and 3D, evaluated in the x–y plane for three different shear rates, are compared in Figure 3. The distributions are computed using equations (2) and (3), while the 2D orientation tensor components are derived following the formulation given in [1]. It can be observed that, for sufficiently large shear rates, the 2D and 3D distributions exhibit very good agreement. However, at lower shear rates, noticeable differences remain due to the intrinsically three-dimensional structure of the orientation distribution.

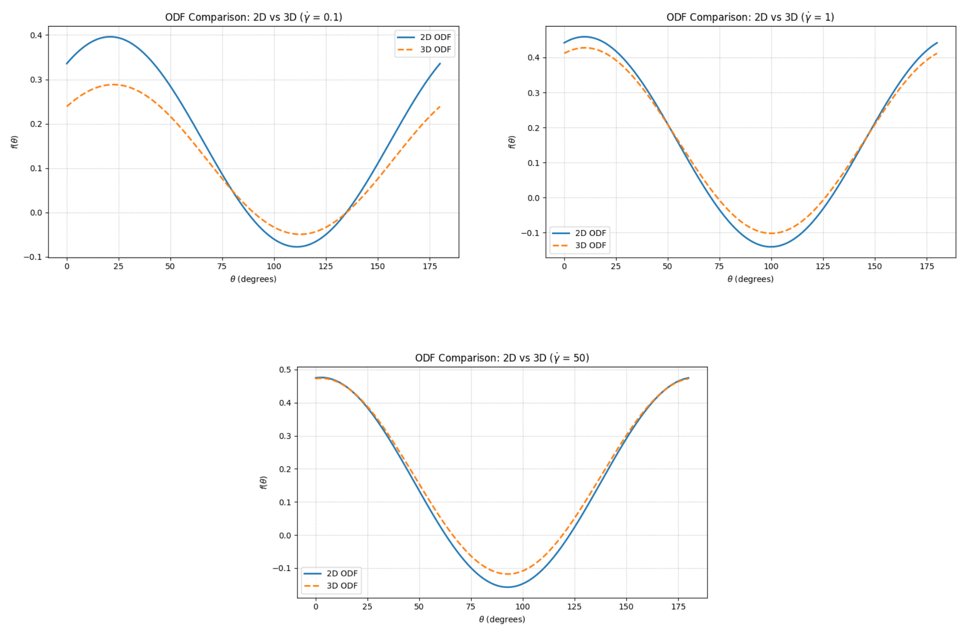

Figure 3: Comparison of the 2D and 3D orientation distribution functions as a function of the angle in the x-y-plane for three different shear rates: $\dot{\gamma} = 0.1,\ 1,\ 50\ (\mathrm{s}^{-1})$.

5 Conclusions and outlook

In this work, the quadratically closed Folgar–Tucker equation (FTE) for planar flows has been solved analytically, providing explicit expressions for all components of the orientation tensor. The solution reveals the essential structure of orientation dynamics in planar velocity gradients. In particular, the out-of-plane components A_{13} and A_{23} decay exponentially, while A_{33} approaches A_{22} in the long-term limit. As a result, the orientation tensor ultimately contains only two independent components.

However, this reduction does not imply that the dynamics become two-dimensional. Since $A_{33} \neq 0$, the orientation tensor does not collapse onto the 1–2 plane. A reconstruction of the orientation distribution confirms that the resulting probability density deviates noticeably from the corresponding 2D approximation. The planar flow problem therefore remains intrinsically three-dimensional, even though the velocity gradient itself is confined to a plane.

The analytical solution also demonstrates that the steady-state orientation is highly sensitive to the shear rate. At very low shear rates, the solution remains nearly isotropic and fully three-dimensional. In contrast, at sufficiently large shear rates, it evolves toward a strongly aligned, effectively one-dimensional configuration. These limiting behaviors can be quantified precisely using the analytical expressions.

Beyond its theoretical significance, the analytical solution provides a rigorous benchmark for validating numerical methods for fiber-suspension flows. Building on this foundation, our future work will focus on developing and testing improved closure models, extending the methodology to more complex geometries and flow conditions, and incorporating newly proposed formulations for fiber-orientation dynamics.

Acknowledgements. The authors gratefully acknowledge the support provided by the Klaus Tschira Stiftung.

References

[1] A. Winters, C. Papenfuss and M. Karow, Benchmarking solutions of the Folgar–Tucker-equation and its reduction to a linear problem for non-linear closure forms, *J. Non-Newtonian Fluid Mech.* 310 (2022), 104922.

[2] C.L. Tucker, *Fundamentals of Fiber Orientation*, Carl Hanser Verlag, 2022.

[3] S.G. Advani and C.L. Tucker, The use of tensors to describe and predict fiber orientation in short fiber composites, *J. Rheol.* 31 (1987), 751-784.

[4] S. Hess, *Integral Formulae and Distribution Functions*, pp. 199-238, Springer International Publishing, Cham, 2015.

[5] G. Jeffery, The motion of ellipsoidal particles immersed in a viscous fluid, *Proc. R. Soc. London, Ser. A* 102 (1923), 161-179.

[6] K. Breuer, M. Stommel and W. Korte, Analysis and evaluation of fiber orientation reconstruction methods, *J. Compos. Sci.* 3 (2019), 67.

[7] D.A. Jack and D.E. Smith, Assessing the use of tensor closure methods with orientation distribution reconstruction functions, *J. Compos. Mater.* 38 (2004), 1851-1871.

[8] J.K. Bauer and T. Böhlke, On the dependence of orientation averaging mean field homogenization on planar fourth-order fiber orientation tensors, *Mech. Mater.* 170 (2022), 104307.

[9] C.L. Tucker, J.G. O'Gara, and J. Wang, An objective model for slow orientation kinetics in concentrated fiber suspensions: Theory and rheological evidence, *J. Rheol.* 52 (2008), 1179-1199.

[10] M. Doi, Molecular dynamics and rheological properties of concentrated solutions of rodlike polymers in isotropic and liquid crystalline phases, *J. Polym. Sci. Polym. Symp.* 19 (1981), 229-243.

[11] T. Karl, D. Gatti, B. Frohnapfel and T. Böhlke, Asymptotic fiber orientation states of the quadratically closed Folgar–Tucker equation and a subsequent closure improvement, *J. Rheol.* 65 (2021), 999-1022.